

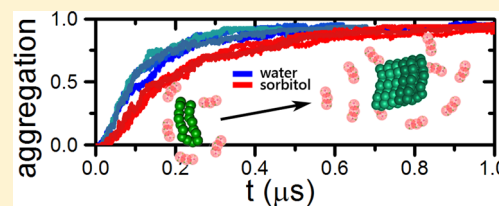
Osmolyte Induced Changes in Peptide Conformational Ensemble Correlate with Slower Amyloid Aggregation: A Coarse-Grained Simulation Study

Shahar Sukenik,[†] Liel Sapir, and Daniel Harries*

Institute of Chemistry and the Fritz Haber Research Center, The Hebrew University, Jerusalem 91904, Israel

S Supporting Information

ABSTRACT: Stabilizing osmolytes are known to impact the process of amyloid aggregation, often altering aggregation kinetics. Recent evidence further suggests that osmolytes modify the peptide conformational dynamics, as well as change the physical characteristics of assembling amyloid fibrils. To resolve how these variations emerge on the molecular level, we simulated the initial aggregation steps of an amyloid-forming peptide in the presence and absence of the osmolyte sorbitol, a naturally occurring polyol. To this end, a coarse-grained force field was extended and implemented to access larger aggregate sizes and longer time scales. The force field optimization procedure placed emphasis on calibrating the solution thermodynamics of sorbitol, the aggregating peptide in its monomeric form, and the interaction of both of these components with each other and with water. Our simulations show a difference in aggregation kinetics and structural parameters in the presence of sorbitol compared to water, which qualitatively agree well with our experimentally resolved aggregation kinetics of the same peptide. The kinetic changes induced by sorbitol can be traced in our simulations to changes in monomer conformations resulting from osmolyte presence. These translate into changes in peptide conformations within the aggregated clusters and into differences in rates of monomer nucleation and of association to formed fibrils. We find that, compared to pure water as solvent, the presence of sorbitol induces formation of more aggregates each containing fewer peptides, with an increased tendency toward parallel interpeptide contacts.



INTRODUCTION

Under conducive conditions, many proteins and peptides spontaneously aggregate into ordered amyloid fibrils.^{1–3} Importantly, the early aggregates of certain amyloid forming peptides are associated with several devastating diseases, motivating numerous studies aimed at understanding the kinetics and thermodynamics of the onset of amyloid aggregation.^{4–6} Osmolytes, also called chemical chaperones, are naturally occurring small molecules that are found at high concentrations in cells. Their role in stabilizing the proteome under conditions of environmental stress is well documented.^{7,8} Moreover, the ubiquitous favorable action of osmolytes on protein stability and activity,^{7,9–12} as well as their widespread use by different cells and organisms,^{13,14} makes them a viable therapeutic option. Indeed, several *in vivo* and *in vitro* studies have shown that amyloid aggregation is inhibited, and in some cases even reversed, in the presence of polyol osmolytes.^{15–18} Interestingly, there are indications that osmolytes may, in addition, alter the morphology of the formed fibrils, thereby affecting their physical characteristics such as fibril brittleness.^{19–22} However, the molecular mechanism of osmolyte action on amyloid formation is not fully understood.

Recently, we have experimentally determined the effect of several polyol osmolytes on the amyloid aggregation of met16, a 16 residue β -hairpin peptide.^{19,23} Of the polyols tested, sorbitol showed the largest effect on met16 aggregation, evidenced in the slowing of the nucleation time in comparison

to aggregation in buffer and by the increased amount of monomers that underwent fibrillation. Analysis of these experimental results with the aid of a kinetic model^{19,24} further suggested that the fibril-monomer pseudodissociation constant, $K_D = k_{off}/k_{on}$, decreases as sorbitol concentration increases. In contrast, the rate constant for fibril breakage, k_b , did not change in the presence of the osmolyte.¹⁹

Experimentally, probing the processes that lead to amyloid aggregation is plagued by many difficulties arising from the complexity of this stochastic, multiprotein association reaction. Molecular dynamic simulations (MD) have emerged as a useful technique to compliment experimental data and help decode the process of amyloid aggregation at the molecular level.^{25–27} Indeed, simulations have been used extensively in recent years to address specific steps in the aggregation process.^{25,27–30} However, the complexity of the process, the long time scales involved, and the collective nature of aggregation require simulations that include a large number of aggregating molecules and long time scales. In addition, simulations of the initial stages of the aggregation process require not only an accurate description of the association process but also a faithful representation of the conformational landscape of single proteins or peptides. Thus, simulations have been able to probe mainly isolated events in the extended process of

Received: July 9, 2015

Published: October 27, 2015

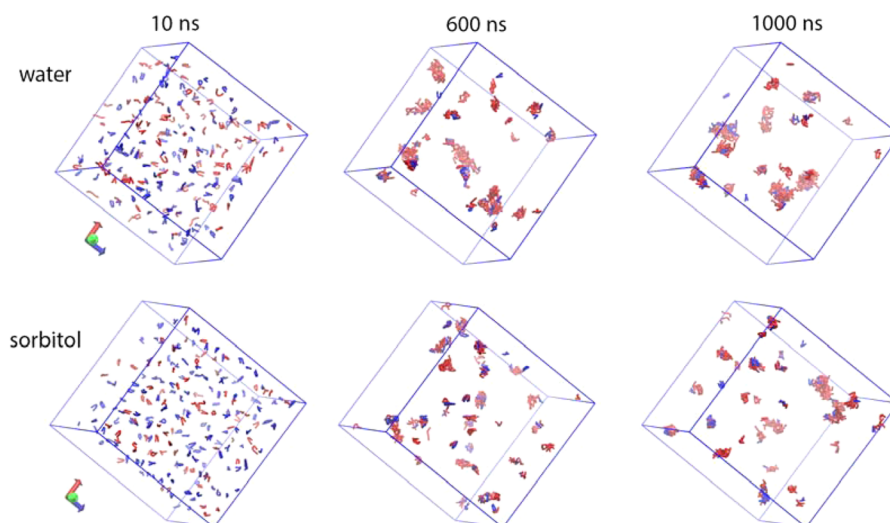


Figure 1. Representative snapshots from the time evolution of aggregation simulations. Colors represent β -hairpin (folded, blue) and unfolded (red) peptides. Clusters are formed over the course of $1 \mu\text{s}$. The presence of sorbitol promotes the formation of a larger number of smaller clusters. The peptides in these clusters show a higher tendency toward the β -sheet conformation of the monomer. Simulation boxes have an edge $\sim 34 \text{ nm}$ long.

amyloid formation and often involve specially tailored force fields or implicit solvents.^{29,31,32} Beyond these complications, simulations of aggregation in the presence of osmolytes must reliably account for interactions between water, osmolyte, and protein. Ultimately, such simulations require the use of force fields that allow access to long time scale dynamics of large systems. Several coarse-grained (CG) MD force fields have been developed over the past decade to address such issues.^{25,29,32–34} For describing biological macromolecules in solution, the MARTINI force field is a promising choice since it has been parametrized using thermodynamic data and has successfully reproduced experimental variables in relatively complex solutions.^{35–37}

Here we develop, validate, and implement a CG model to simulate the initial stages of peptide aggregation in the presence and absence of sorbitol. The implemented model is based on the MARTINI force field with further parametrization to account for polyol osmolytes. The modified force field quantitatively reproduces several experimentally determined kinetic and thermodynamic properties of the met16 peptide and its aggregation process in the presence and absence of sorbitol. To allow accurate simulations of the folding and unfolding of the coarse-grained model peptide, pseudodihedral angles from an all-atom replica-exchange molecular dynamics (REMD) simulation are incorporated into the CG force field. In parametrizing the sorbitol model, we use an extensive set of experimental data that includes partial molar volumes and preferential interaction coefficients. Finally, the interaction between sorbitol and met16 is calibrated against the experimentally determined change in folding free-energy of the peptide monomer, which reflect changes in peptide preferential hydration. The resulting accessible time scale and size of our CG simulations afford unique insights into the first microsecond of the aggregation process, corresponding to the time required for prefibrillar aggregate formation, and allow us to characterize the differences between the initial stages of the aggregation process in water and in the presence of sorbitol.

Our simulations, shown at representative times for water and sorbitol solution in Figure 1, demonstrate that sorbitol's presence indeed impacts the aggregation process. On the

single peptide level, the presence of sorbitol shifts the monomer population from the unfolded toward the folded ensemble, with a particular tendency to decrease the population of highly extended conformations within the unfolded ensemble. The presence of sorbitol changes both the kinetics of peptide aggregation and the resulting conformations of peptides in clusters. Specifically, sorbitol decreases the rate of monomer association to clusters as well as the rate of nucleation. Sorbitol also increases the number of aggregates and decreases their average size compared to water, as seen in Figure 1. Finally, sorbitol induces order in formed clusters, favoring a “head-to-head” peptide orientation. These findings suggest that the effect of sorbitol on amyloid aggregation kinetics and the conformations of prefibrillar aggregates occur at the level of the folded/unfolded monomeric conformations that become more/less prone toward aggregation in the presence of the osmolyte.

MODEL AND FORCE FIELD CALIBRATION

Peptide Force Field Calibration. The met16 peptide, shown schematically in Figure 2A, is composed of 16 amino acids, with the sequence Ac-KKYTVSINGKKITVSI. This peptide, originally developed as a DNA binding motif,³⁸ has been extensively studied by us and others, both experimentally^{39–43} and in simulations,⁴⁴ as a model of peptide folding and aggregation. Met16 is a two-state folder, with an experimentally resolved folding free energy of $\Delta G \approx -1.2 \text{ kJ/mol}$ in aqueous solution buffered at neutral pH and at room temperature.⁴³ To simulate the folding/unfolding equilibrium characteristics of the monomeric peptide in the CG representation, we adopted the methodology developed by Seo et al.,⁴⁵ whereby dihedral angle potentials are inserted into the CG model based on all-atom (AA) REMD simulations. This procedure is required because within the original MARTINI protein force field³⁶ peptides retain a rigid secondary structure and dihedral angles are not included. Fixed dihedral angles would be inappropriate for the process we model, since each peptide would then retain its initially set conformation, and would not be able to dynamically

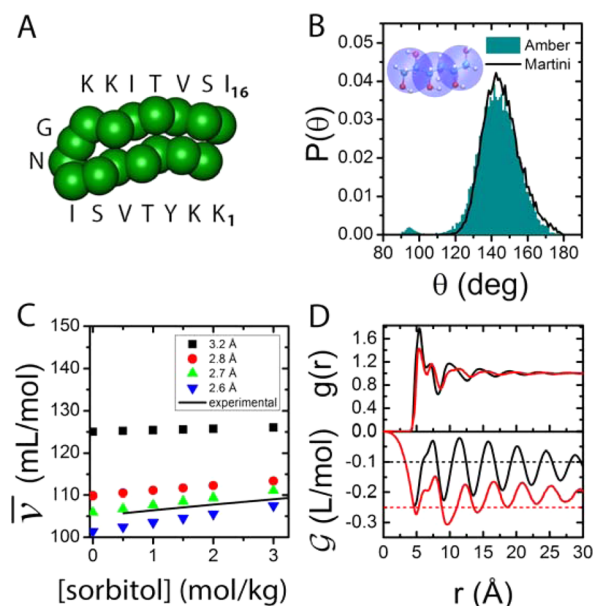


Figure 2. Comparisons of calibrated coarse-grained models to experiment and all-atom simulations. (A) CG met16 model peptide (showing backbone beads only) in a folded conformation. (B) Optimized angle distribution between the three CG spheres (MARTINI), compared with the AA (Amber) simulations. Inset shows the CG sorbitol model (blue spheres) overlapping the all-atom model of sorbitol. (C) Partial molar volumes as a function of sorbitol concentration for various bond lengths. The final selected length for subsequent simulations based on the fit to experimental data was 2.7 Å. (D) Preferential interaction of CG sorbitol and water. The distance r is measured between water beads and sorbitol center-of-mass. (Upper panel) The radial distribution function for water (black) and sorbitol (red) around a sorbitol molecule. (Lower panel) The Kirkwood–Buff integrals for sorbitol–water and sorbitol–sorbitol distributions defined in eq 2, corresponding to the radial distributions shown in the upper panel. The limiting values for these integrals are compared to the experimental preferential interaction values, shown as dashed lines.

interchange between the different forms of the peptide: folded, unfolded (or misfolded), and aggregated.²³

Probability distributions of the dihedral angles were obtained from the last 300 ns of a 500 ns AA-REMD simulation, and the CG dihedrals were taken as the pseudodihedral angles between the centers of mass of the backbone heavy atoms (C_α , N, C, and O) of four neighboring residues (See Sections S1–S2 in the Supporting Information (SI) for additional details on the REMD simulation.). From these distributions, the free-energy landscape for each of the 13 dihedral angles is obtained through the relation $U_i = -kT \ln P_i$, where k is the Boltzmann constant, T is the absolute temperature, U_i is the potential of mean force of dihedral angle i , and P_i is the probability density of that angle. Then, U_i was fit to the functional form given by $U(\theta) = \sum_{m=1}^n k_m [1 + \cos(n_m \theta - \theta_m)]$, where typically the number of terms in the summation, $n = 6$, but may be as high as 10, depending on the complexity of the dihedral probability distribution. The determined values of k_m , n_m , and θ_m are used in the dihedral potential of the backbone beads of the CG peptide, and a 500 ns simulation of a single peptide in MARTINI water is run to find the dihedral angle distribution of a single peptide in the CG model. While a least-squares fitting procedure produces good fits to the energy landscape of a single dihedral, coupling between neighboring dihedral angles

affects the final distribution and requires a user-guided iterative process to match the final angle distributions. After ~ 30 such iterations, we arrived at a CG dihedral angle distribution for the peptide that is in good agreement with the AA analogue (Figure S3). The calibrated peptide was then simulated in explicit MARTINI water at 300 K for 10 μ s to extensively probe the conformational landscape of the peptide. While a larger part of the unfolded conformational space is sampled in the CG representation (which may be the result of more extensive sampling in the CG model, or a “smoother” energy surface in the CG representation), the position of the maxima in the end-to-end peptide distance, as well as saddle points and overall shape of the AA-REMD simulations, is well preserved in the CG representation (shown in Figure S4). All bonded parameters for the met16 CG model are available in the SI, appendix 1.

Sorbitol Force Field Calibration. The calibration scheme for the CG sorbitol model was as follows. We first selected a MARTINI bead type that closely matched the chemical characteristics of the polyol groups. This is important because the choice of bead parameters defines the sorbitol self-interaction and its interaction with water beads simulated in the binary solutions. Once the bead was selected, we optimized internal sorbitol angles, based on AA simulations, and finally adjusted bond lengths to match experimental partial molar volumes of sorbitol. With these parameters optimized, we turned to adjust the sorbitol interactions with peptide moieties. Importantly, the calibration may require an iterative process since changes to any single parameter we mention above is coupled to other optimized parameters. In our case, retesting the observables after the first round of the described calibration showed no appreciable change in angle distribution or partial molar volume of our model. All data shown is taken from simulations of the final selected model, whose parameters are available in the SI appendix 2.

The CG sorbitol model we developed, shown in the inset of Figure 2B, includes three MARTINI beads, each representing 4 heavy atoms (two carbon atoms and two hydroxyl oxygen atoms) joined by two equidistant bonds. The three beads are connected by a single angle, defined as the angle between the centers of mass of each 4 bonded heavy-atoms in an AA simulation, which was used to calibrate the sorbitol CG model. Here, the AA simulations of sorbitol are based on a simulation with the Amber GLYCAM06 force field,⁴⁶ averaged over the last half of a 200 ns MD simulation. Details of the calculations and model used are available in Section S1 in the SI. The resulting distribution of CG bond angles is shown and compared with AA results in Figure 2B.

Once the angle is adjusted, we turn our attention to the bond length between beads. The partial molar volume, \bar{v} , is a parameter that sensitively depends on the composition of the solution as well as the dimensions and interactions of the molecules and is a good measure for the effective size of the cosolute. We thus modified bond lengths in order to match experimental \bar{v} values for sorbitol aqueous solutions. To measure this property in simulations we used CG simulations of a series of binary solutions with concentrations 0.5, 1.0, 1.5, 2.0, and 3.0 mol/kg and calculated \bar{v} from the relation

$$\bar{v}(x_s) = \left(\frac{\partial \bar{V}}{\partial x_s} \right)_{P,T} \quad (1)$$

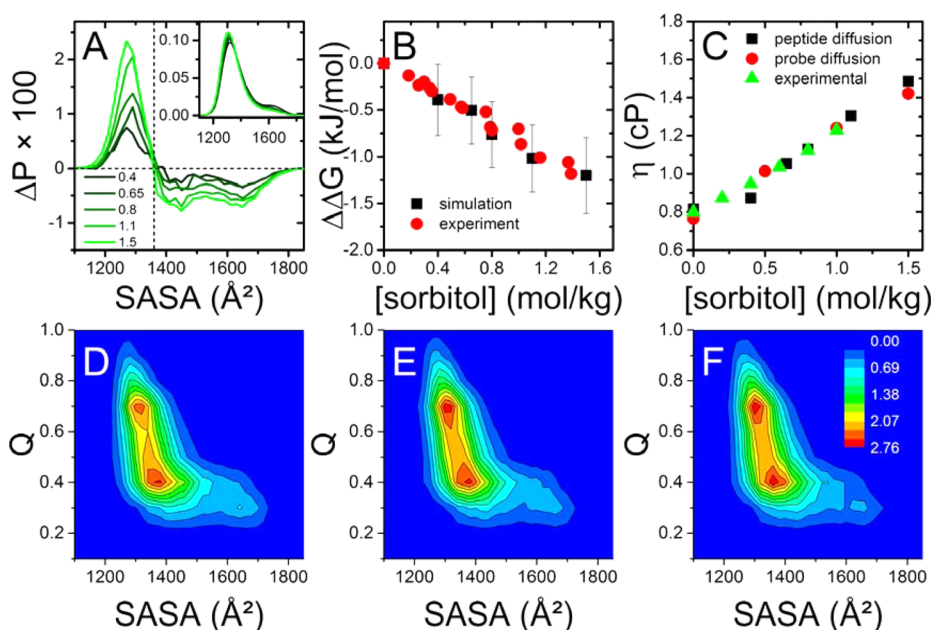


Figure 3. Stability of met16 in the presence and absence of sorbitol. (A) The difference between peptide SASA probability distribution in sorbitol solution and in water for various sorbitol concentrations shows a distinct threshold value between increased (left of vertical dashed line, folded) and decreased (right of the line, unfolded) populations. Inset shows SASA distributions for all concentrations used. (B) The change in free energy of peptide folding with sorbitol concentration derived from simulations and experiments, compared to folding in water. (C) Sorbitol solution viscosity in experiment and simulations. Viscosity was measured using the diffusion of a sphere (red circles). The diffusion of the peptide was scaled by a single effective radius to match the same viscosity (black squares) for varying concentrations of sorbitol. Results are compared with experimental viscosity measurements⁵⁸ (green triangles). (D–F) Two-dimensional conformational distribution of the fraction of β -hairpin contacts, Q , and the backbone SASA of CG met16 in the presence of water (D), 0.65 mol/kg sorbitol (E), and 1.1 mol/kg sorbitol (F). Probability density scale (in percent probability) is shown in panel F. The difference between sorbitol concentrations is most notable in the high SASA ($>1500 \text{ \AA}^2$) tail of the distribution (see also Figure S7).

where \bar{V} is the total box volume per mole of all components, and x_s is the mole fraction of sorbitol. Partial molar volumes in the simulation are compared with experimentally known values shown as the solid line in Figure 2C, allowing to select the model that best fits experiments.⁴⁷ Thus, sorbitol bond lengths were set at 2.7 Å to give the smallest deviation from experiments over the concentration range used in our simulations. All MARTINI sorbitol parameters are available in the SI, appendix 2.

Osmolyte-Water Interaction. Once bonded parameters have been assigned, the nonbonded parameters can be calibrated. Note that, as previously stated, both bonded and nonbonded parameters can affect partial molar volumes, so that proper calibration of both bonded and nonbonded parameters may require rechecking after parametrization. Initial nonbonded interactions are defined by the bead selected for sorbitol from the set of default MARTINI bead types. Our starting point was the P4 type bead that is also used to represent water. This choice was motivated by the fact that the sorbitol molecule contains many hydroxyl groups; we, therefore, expected that an appropriate starting point to represent hydrogen-bond forming osmolyte moieties would be beads that are similar to water. In addition, the P4 bead has previously been used in MARTINI models to represent the polyol head groups of phosphatidylglycerol lipids.³⁵ Since each bead in the sorbitol model represents the same 4 heavy atoms (i.e., two carbon atoms and two oxygen atoms), calibration of only a single bead type is required.

To test the interactions between sorbitol and water in binary solutions, we used the Kirkwood–Buff (KB) theory of solutions.^{48,49} Specifically, we compared experimentally avail-

able KB integrals to those derived from simulations. The KB integrals, defined as

$$\mathcal{G}_{ij} = \int_{r=0}^{\infty} (g_{ij}(r) - 1) 4\pi r^2 dr \quad (2)$$

are spatial integrals over the radial distribution functions (RDF, $g(r)$) of the components i and j . The RDF of sorbitol–sorbitol and sorbitol–water beads (subscripts ss and sw , respectively) is shown in Figure 2D. The figure also shows the resulting integration presented as a function of r , which represents the limit of integration distance from the center of mass of a reference sorbitol molecule. Note that as $r \rightarrow \infty$, the value of \mathcal{G} approaches a limiting value, \mathcal{G}^∞ . This limiting value can be derived experimentally by means of osmometry or using other techniques^{49,50} and shows good agreement with our simulated values. This is to be expected, as the KB integrals in a binary mixture often closely correspond to the molecular volume of a species, and these were already calibrated as described in the previous section.

The undulations seen in the KB integrals (Figure 2D, lower panel), persisting even at rather large distances, are characteristic of Lennard-Jones liquids.⁵¹ Fitting the bulk region ($r > 15 \text{ \AA}$) to a damped sine function of the form $\mathcal{G} = \mathcal{G}^\infty + A \exp(-r/r_0) \sin(\pi r/w)$ (where \mathcal{G}^∞ , A , r_0 , and w are fit parameters) allows estimation of the convergent value of the integral, \mathcal{G}^∞ . In our CG simulations we found $\mathcal{G}_{sw}^\infty = -0.09 \pm 0.04 \text{ L/mol}$ and $\mathcal{G}_{ss}^\infty = -0.22 \pm 0.01 \text{ L/mol}$ for 1.5 mol/kg sorbitol solution, compared with -0.1 L/mol and -0.25 L/mol respectively, known from experiments.⁵²

An important consequence of properly calibrating the model to fit the KB integrals is a good match to solution osmotic pressure. To compare the osmotic pressure in our simulations with the experimental values for sorbitol solutions, we make use of a range of binary solution simulations, with CG sorbitol concentrations ranging between 0.1 to 1.5 mol/kg, as described in Section S3 of the SI. This comparison demonstrates how the CG model well reproduces the osmotic pressure, a fundamental thermodynamic property of this sorbitol–water binary solution.

Cosolute–Peptide Interactions in Ternary Mixtures.

The interaction of sorbitol with the peptide monomer is manifested in the concentration-dependent effect of sorbitol on the folding free-energy of the peptide, ΔG_{fold} . We have previously experimentally quantified this effect and its extent for met16 through the m -value,^{40,43} defined as $m = d\Delta G_{fold}/d[\text{cosolute}]$.⁵³ We therefore use the m -value to calibrate the interaction between the sorbitol model and the peptide. In our experiments with sorbitol and the met16 peptide, we find $m \approx -0.9 \pm 0.1 \text{ kJ mol}^{-1}(\text{mol/kg})^{-1}$.⁴³ The interactions between sorbitol, peptide, and water were calibrated by adjusting the Lennard-Jones interaction between the sorbitol beads and the peptide backbone, leaving other interactions (namely side chain–sorbitol and water–peptide interactions) at their default MARTINI values for P4 beads. This choice is supported by the studies of Bolen and others, which have shown that the major contribution to exclusion of osmolytes from peptide surfaces stems from osmolyte–backbone interactions.^{10,52,54,55} Another reason to use these interactions for calibration is that backbone surface exposure changes dramatically between unfolded and folded ensembles compared to other moieties, thus these interactions are most strongly affected by changes in solvent interactions (Figure S8).

To determine how sorbitol alters the peptide monomer's folding free energy, we evaluate the folding equilibrium constant, $K_{eq} = \exp(-\Delta G_{fold}/kT)$, in our simulations by counting folded and unfolded instances according to a single selection criterion at all sorbitol concentrations. Since we parametrize the model according to the extent of cosolute exclusion from the peptide surface area, we used the backbone solvent-accessible surface area (SASA) as a relevant structural parameter for differentiating folded from unfolded conformations. The threshold value separating folded and unfolded SASA values was determined using several concentrations of sorbitol (0.4, 0.65, 0.8, 1.1, and 1.5 mol/kg). The SASA distribution curves are shown in the inset of Figure 3A. Expectedly, as sorbitol concentrations increase the peak with the lower SASA (representing the folded ensemble) grows and the peak with the higher SASA is depressed. The trend becomes even more apparent when we subtract the probability distribution in the presence of sorbitol from the probabilities in water, ΔP . Figure 3A shows a region where ΔP increases, and a region where it decreases. Importantly, all curves intersect at a single point, where $\Delta P \approx 0$. This value (in this case, SASA = 1360 Å²) is selected as the threshold between folded and unfolded conformations. We suggest this computational cosolute-perturbation method as a general way to obtain folded/unfolded population thresholds in protein and peptide simulations. Notably, this method requires no prior assumptions on the peptide or protein conformational ensemble.

The folding equilibrium constant and the related free energy are then derived through the ratio of the number of frames that show peptide conformations above and below the determined

threshold. We verify the convergence of the values for the equilibrium constant by bootstrapping.⁵⁶ The linear decrease in the folding free-energy due to sorbitol, $\Delta\Delta G = \Delta G_{fold,s} - \Delta G_{fold,w}$ as a function of sorbitol concentration, Figure 3B, indicates that the polyol CG model is indeed excluded from the peptide surface and that the changes in preferential hydration between folded and unfolded conformations remain constant at all tested concentrations. The slope of $\Delta\Delta G$ versus sorbitol concentration, shown in Figure 3B, represents the simulation-obtained m -value, which closely matches the experimental one. We also compared results from an alternative method to obtain the m -value that relies on KB integrals to determine the preferential interaction coefficients, as described in Section S4 of the SI. Both methods gave the same results within statistical error. Nonbonded parameters for the bead type used for the sorbitol model are available in the SI, appendix 3.

Solution Viscosity. To interpret the effect of sorbitol on kinetics of aggregation in our simulations, we first establish the viscosity of the CG sorbitol solution and compare these to experimental values. To this aim, we performed several simulations of different binary solution concentrations, and the diffusive displacement of a spherical probe with a radius of 3.7 Å was measured in a 2 μs CG simulation. The diffusion coefficient, D , was evaluated from the mean-square displacement of the probe molecule using the `g_msd` module of the GROMACS suite.⁵⁷ This diffusion constant is then related to the solution viscosity η through the Stokes–Einstein relation

$$\eta = kT/(6\pi Dr) \quad (3)$$

where r is the probe radius. We find a surprisingly good agreement with the experimental⁵⁸ viscosity of these binary solutions over a wide range of sorbitol concentrations, Figure 3C. We then used this viscosity value and the diffusion constant from our simulations to calculate an effective hydrodynamic radius of $r = 16 \text{ Å}$ for the simulated peptide. Overall, we find that in both experiments and in CG simulations the effective viscosity of sorbitol solutions increases by a factor of ~ 1.5 in a 1 mol/kg sorbitol solution compared to water.

■ STRUCTURAL AND KINETIC ANALYSIS

Changes to Conformational Landscape. We examine the changes to the conformational landscape of met16 induced by sorbitol by looking at the 2D probability distribution of backbone SASA and of Q ,⁵⁹ a parameter that quantifies the amount of β -sheet-like native contacts present in the peptide, defined by

$$Q = \frac{1}{N} \sum_{i=1}^N \sum_{j=i+2}^N \frac{\delta_{ij}}{(1 + e^{r_{ij}-r_0})} \quad (4)$$

Here, N is the number of residues on the peptide, r_0 is the cutoff distance for a contact (set at 6 Å), r_{ij} is the distance between residues i and j for a given frame, and $\delta_{ij} = 1$ when residues i and j are in contact in the β -hairpin state (shown in Figure 2A), and $\delta_{ij} = 0$ otherwise. These two parameters (SASA and Q) are largely orthogonal to each other, as can be seen from the L-shaped distribution map in Figure 3D–F, giving a good representation of the conformational landscape. While the overall features of the distribution remain constant with increasing sorbitol concentrations, the conformations with high SASA and low Q are depleted at high sorbitol concentration. This is shown more clearly in the difference between the distributions in water and in the presence of

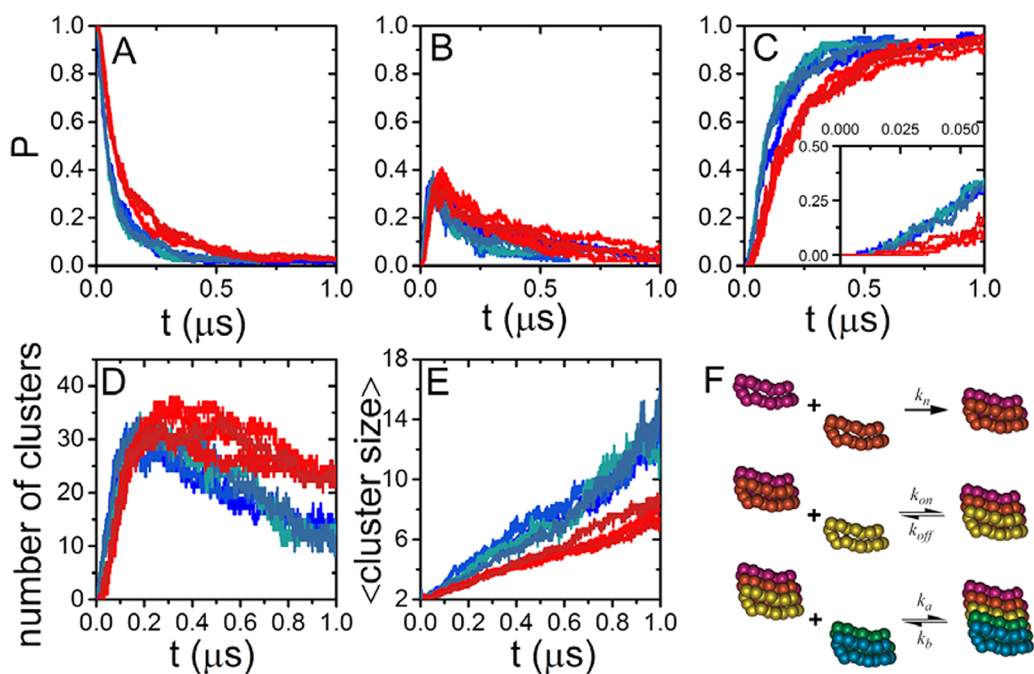


Figure 4. Kinetics of met16 aggregation and cluster sizes in the presence of water (4 trajectories, blue) and in 1 mol/kg sorbitol solution (3 trajectories, red). Probability of finding a peptide in a monomeric state (A), as a dimer (B), or as a higher-order oligomer (C). Inset zooms in at short times to highlight differences in lag time. (D) Total number of clusters as a function of time. (E) Average cluster size as a function of time. (F) Scheme of the kinetic model used to analyze the results, showing from top to bottom: nucleation, monomer attachment/detachment to/from fibrils, and fibril association and breakage.

Table 1. Kinetic Rates Obtained by Model Fits to Simulation Data and from Experimental Data

rates		water ^b	sorbitol ^b	simulation water/sorbitol	experimental water/sorbitol ¹⁹
k_{on} (ns ⁻¹ M ⁻²)	monomer-to-fibril attachment rate	0.7 ± 0.1	0.43 ± 0.05	1.6	4.2
$k_{off} \times 10^7$ (ns ⁻¹ M ⁻¹)	monomer-from-fibril detachment rate	400 ± 300	3 ± 1	133	7.5
k_n (ns ⁻¹ M ⁻²)	nucleation (dimerization) rate	0.44 ± 0.06	0.30 ± 0.03	1.5	1.8
k_a (ns ⁻¹ M ⁻²)	fibril-to-fibril attachment rate	0.5 ± 0.3	0.5 ± 1	1	N/A ^a
$k_b \times 10^7$ (ns ⁻¹ M ⁻¹)	fibril breakage rate	3 ± 2	2 ± 2	1.5	0.06

^aNot included in experimental data fit. See SI, Section S6 for details. ^bErrors are standard deviations from 5 repeats of the fit starting from random initial guesses, for each of the replica runs (20 and 15 repeats for water and sorbitol, respectively).

sorbitol, SI Figure S7. The fact that sorbitol stabilizes or destabilizes conformations according to their backbone SASA is in line with our calibration and with the expected mechanism for sorbitol action: the conformations with high SASA are destabilized mainly due to effectively repulsive interactions between sorbitol and peptide backbone. Thus, as sorbitol concentrations increase, conformations are shifted even within the unfolded ensemble from high-SASA conformations to compact, misfolded, low-SASA conformations. We suggest that these subtle changes to the conformational landscape importantly contribute to the changes in aggregation kinetics due to the presence of sorbitol, as we later discuss.

Aggregation Kinetics. All coarse-grained multi-peptide simulations of met16 aggregations consisted of 216 CG peptides. The peptides, with random initial conformations, were initially constrained, and the solvent was allowed to equilibrate around them for 10 ns. The equilibrated system was used as the starting point ($t = 0$), and multiple trajectories for each condition (in water and in 1 mol/kg sorbitol) were run for statistical significance. Complete details of the simulations' parameters are available in the SI, section S1. The kinetics of aggregation were followed by counting clusters in each frame based on a minimal distance criterion ($r < 6$ Å) between any

two beads from different peptides. The time-resolved probabilities of finding a peptide as a monomer, dimer, or higher order oligomer are shown in Figure 4A, B, and C, respectively.

In agreement with experiments of met16 aggregation,²³ the presence of sorbitol acts to slow the rate of monomer consumption, resulting in longer aggregation lag times (see Figure 4C inset). To further compare our simulations with the experimental analysis,¹⁹ we fit the set of simulated kinetic curves, including probabilities for peptides to be monomers, dimers, or larger clusters (shown in Figure 4, panels A–C), to a master equation that we have previously used to describe the experimental aggregation process. This master equation uses five rate constants, shown schematically in Figure 4F and specified in Table 1. The details of this master equation are given in the SI, Section S6. We then used a fitting procedure to find rate constants that minimize the sum of squared deviations between the analytic and simulated curves. The average values for each rate constant are given in Table 1.

The values determined for the five kinetic constants indicate that several of these are impacted by the presence of sorbitol in solution. First, both monomer attachment and detachment rates are slowed in the presence of sorbitol. However, while k_{on}

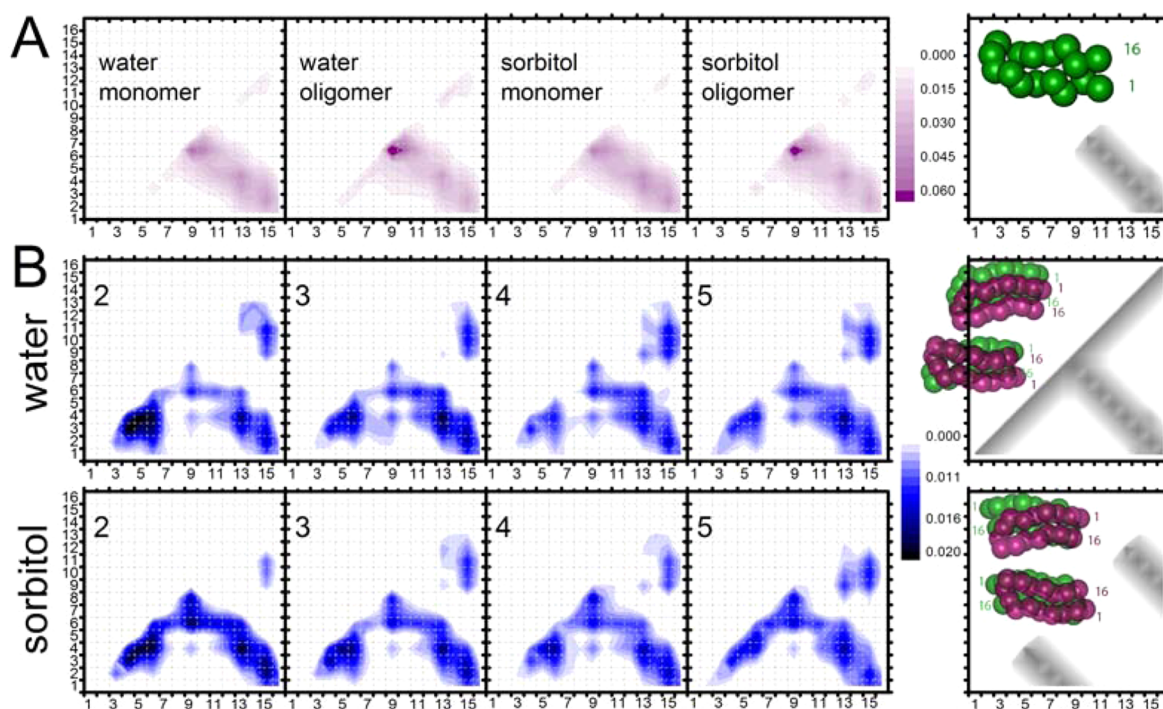


Figure 5. Peptide residue contact maps in clusters of various sizes. (A) Probability for intrapeptide contacts between residues that are at least 4 amino acids apart in sequence in water and sorbitol solution. For comparison the map on the far right represents an idealized β -hairpin contact map. (B) Probability for interpeptide contacts. The top half of the panel shows the probabilities in the presence of water and the bottom half in the presence of 1 mol/kg of sorbitol. The numbers represent cluster size. Maps on the far right represent idealized contact maps for parallel (head-to-head, top) versus antiparallel (head-to-tail, bottom) alignments.

is slowed by a factor of ~ 1.5 (which closely matches the change in solution viscosity in the presence of sorbitol, Figure 3C), the detachment rate, k_{off} is slowed by 2 orders of magnitude, much larger than the change in viscosity. Thus, our experimental results indicated that the ratio of these rates, $K_D = k_{\text{off}}/k_{\text{on}}$, is smaller in the presence of sorbitol. Yet, while in our experiments the K_D in the presence of sorbitol was smaller than in water by a factor of 2, the simulations show a ca. 80-fold decrease. The larger change in the presence of sorbitol found in simulations may be a result of relatively poor sampling of monomer detachment and is also likely affected by the strong protein–protein interactions known for the MARTINI force field.^{60,61} Moreover, peptide concentrations in our simulations are roughly 30 times higher than in the experiments, which can lead to differences in the kinetic scheme. Indeed, experiments show that aggregation occurs much faster, almost instantly, for met16 at concentrations exceeding 1 mM. Although dissociation events are relatively rare in our simulations, so that relatively large errors should be expected in determining the off-rate, the effect of sorbitol compared with water is apparent and shows the same trends in simulations and experiments (Table 1). Fibril breakage, another rare event in our simulations, shows the opposite trend from our experimental findings. This discrepancy may be a result of processes involving fully formed fibrils that occur on much longer time scales during amyloid aggregation and are not sampled in our simulations. In line with experimental observations, we also find that the nucleation rate, k_n , calculated in simulations is reduced in the presence of sorbitol.

An additional point where aggregation differs in water compared to the presence of the osmolyte is in the total number of aggregates and their sizes, shown in a representative

snapshot in Figure 1 and analyzed in Figure 4D and E. In water, the number of peptide clusters is consistently lower than in the presence of sorbitol. This is especially noticeable at longer times, despite an equal probability for monomers to be part of a cluster in the presence and absence of sorbitol (Figure 4C). This observation is at odds with macromolecular crowding theory, which would predict that the presence of cosolutes will act to decrease the excluded volume taken up by the protein.^{41,62,63} In our case, a push toward volume decrease should favor the formation of a small number of large clusters. Sorbitol, in our simulations, does the opposite and induces the formation of more clusters with less peptides compared to water. Importantly, while the theory of macromolecular crowding has had success in predicting the effect of certain crowding agents on amyloid aggregation,^{62,64,65} it has failed to accurately predict important experimental cases of osmolyte inhibition of amyloid aggregation.^{16,18,23} The differences seen in the simulations in cluster size are in line with what our kinetic predicts: shorter nucleation times and faster monomer association in water lead to faster aggregation and yield larger clusters compared to sorbitol solution.

Structural Analysis of Peptides in Clusters. To link the observed sorbitol effect on the kinetics and thermodynamics of the aggregation process with sorbitol's impact on peptide structure, we compare several structural parameters in the presence and absence of the chemical chaperon. To analyze the conformations that appear in clusters of different sizes, we quantified the intrastrand contact probabilities in both sorbitol and water. Specifically, we counted the total number of contacts for which the distance $r_{ij} < 6 \text{ \AA}$, where i and j are two beads representing two amino acid backbone units, and $j \geq i + 4$. We then determined how these contacts are distributed over the

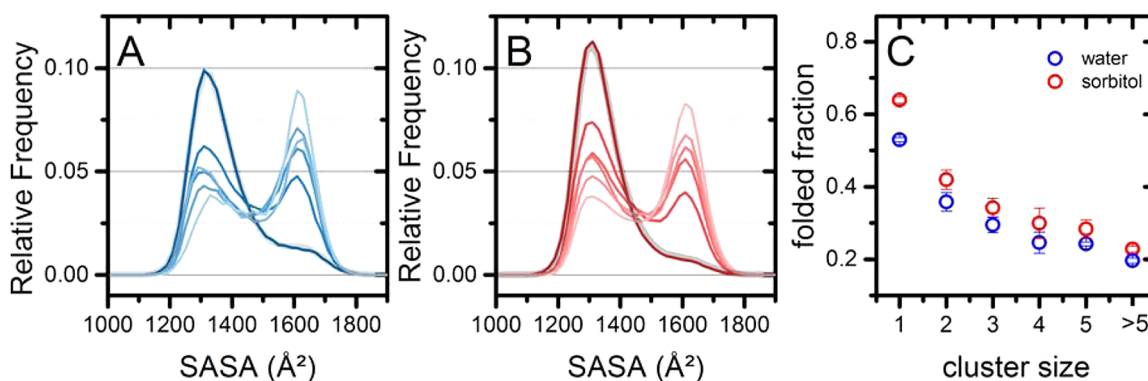


Figure 6. Structural differences of monomers within clusters. Backbone SASA probability distributions in water (A) and 1 M sorbitol (B). As cluster size increases (lighter colors) there is a shift toward unfolded conformations. The gray curve shows the SASA distribution from the simulation of a single monomer under the same solution conditions. (C) Fraction of folded peptides versus cluster size. Error bars are standard deviation between trajectories.

entire trajectory for clusters of various sizes, Figure 5A. We find that the majority of *intra*-peptide contacts lie on the diagonal describing the β -hairpin form of the peptide, where residue 1 is in contact with residue 16, 2 with 15, and so on (see scheme in Figure 2A and 5A). Importantly, this native-like contact probability map does not vary considerably in the presence of sorbitol, nor does it change dramatically as clusters are formed.

To test the arrangements of peptides within clusters, the *inter*-peptide contact probability was determined for various sized clusters. A contact was defined based on the same criterion as intrapeptide contacts. Probabilities were evaluated as fractions of the total number of contacts in clusters of the same size. Figure 5B shows contact probability distributions for dimers through pentamers. In contrast to the intrapeptide contacts, the interpeptide contact maps reveal a different cluster arrangement in the presence and absence of sorbitol. Starting from dimers, and becoming more pronounced as cluster size increases, a trend toward the so-called parallel configuration is observed in the presence of sorbitol, showing better resolved diagonals. To contrast, in water additional antiparallel cluster arrangements exist as well, becoming more pronounced as cluster size increases.

From analysis of the effects of sorbitol on the monomer conformational landscape (Figure 3D–F), we can expect a slightly larger folded population in the presence of sorbitol. To contrast, the folding conformational landscape for peptides in clusters shows a higher population of the unfolded ensemble, both in water and sorbitol solution, Figure 6A and B. These can be quantified to give the folded peptide fraction in different aggregate sizes, based on the same criteria for peptide folding derived for the single (monomer) peptide, as shown in Figure 6C. We find that the transition from monomers to dimers is accompanied by a sharp drop in peptide hairpin folded population. This is in line with a common mechanism for amyloid nucleation derived based on experimental observables, whereby aggregation initiates from an unstructured (or misfolded) conformation, which subsequently templates additional monomers into the misfolded state.¹ This preference toward unfolded peptides in dimers may be a result of an increased surface area for unfolded monomers (the so-called “fly-cast mechanism”)⁶⁶ or alternatively can result from a “dock-lock” mechanism.⁶⁷ Once docking is achieved, the peptide can lock into the correct template but may also be trapped in an unstructured conformation. The extent of these states and their lifetime would depend on solution conditions, including the

presence or absence of osmolyte. We find that in the presence of sorbitol the folded populations remain more preserved in the small clusters, and the trend persists even in clusters larger than 5, where the fraction of folded peptides in sorbitol is still larger than in water, Figure 6C.

These findings provide new insight into the effects of sorbitol on protein aggregation. The impact of osmolytes on isolated monomers appears to be straightforward: its presence shifts the peptide folding equilibrium toward conformations with lower surface area (that results in a linear dependence of the folding free energy on osmolyte concentration, Figure 3B,D–F). This effect of sorbitol and other osmolytes on various proteins and peptides has been observed both experimentally^{7,43,68–70} and in simulations.^{44,71} In contrast, we find that multiprotein processes such as oligomerization are impacted by polyols not only through the change in protein stability but also in the changes in physical and structural characteristics for the formed aggregates, indicative of aggregate polymorphism.^{72,73} Since the difference between sorbitol solution and pure water is derived from the interactions of the osmolytes with the monomeric peptide, we suggest that the effect of sorbitol on protein complexes can be traced back to the relatively small structural changes it induces in the monomeric peptide. Specifically, our results suggest that the aggregation process proceeds differently in the presence of sorbitol due to small changes in the conformational landscape of the attaching monomers, a process reminiscent of the previously observed templated amyloid growth.^{74–76} Thus, a higher tendency toward β -hairpin conformations in sorbitol translates to slower nucleation and monomer attachment rates and leads to a larger concentration of smaller aggregates that retain an overall higher fraction of β -hairpin conformations, as compared to the same process in water alone. We hypothesize that peptides and proteins whose monomeric folding equilibrium constant is more mildly affected by cosolutes (perhaps achievable through rationally designed mutations) will show similar kinetics in water and in the presence of cosolute containing solutions. In addition, it will be interesting to see if denaturants such as urea will promote more rapid, randomly structured aggregation and also increase dissociation constants, since these solutes are thought to increase the SASA of the unfolded state.⁷⁷

CONCLUDING REMARKS

We have presented a CG model to study the effects of the osmolyte sorbitol on the aggregation of a peptide from its initial monomer population. Beyond conclusions concerning the microscopic details of the aggregation process, this study indicates that, despite the known shortcomings of coarse graining, such as inadequately dissecting free energies into entropy and energy, significant and otherwise hard to access information can still be gained from thermodynamically well calibrated CG models.

The effect of sorbitol on peptide folding was calibrated through careful parametrization that maintained close contact with experimental observables. The effect of sorbitol on the peptide conformational ensemble helped us determine the folded and unfolded states in an unbiased way. Moreover, the resulting sorbitol and peptide models quantitatively well reproduced the experimental effect of sorbitol on the free energy of peptide folding. This calibrated force field was then used to simulate the initial stages of amyloid aggregation and to compare this kinetic process with our experimental results in the presence and absence of sorbitol. The main conclusions from the simulations are supported by experiments. Specifically, we found that sorbitol drives monomers to form a larger number of smaller clusters compared to water over the time scales tested here. This is a result of a decrease in the net association rate of monomers to fibrils and a decrease of net nucleation rate in the presence of sorbitol. Further analysis of monomers and clusters indicates that the main structural difference in peptide aggregates in the presence of sorbitol is the stronger propensity for β -sheet folding. This tendency persists significantly in smaller clusters, where exposure of peptides to the surrounding solution is high. In addition, the presence of sorbitol increases the propensity to form parallel interpeptide contacts, compared to water. Taken together, we conclude that the relatively small effect of osmolytes on the folding of a single peptide is propagated and amplified as the monomers self-assemble into aggregates. Most prominently, the net rate for monomer attachment is slowed down not only by increased viscosity but also by a more selective attachment/detachment to clusters (“templating”) seen in the presence of sorbitol. This leads to a greater structural similarity between the attaching monomer conformations and the templating nucleus. It is tempting to speculate that the differences we find in aggregates that form in the presence and absence of osmolytes, reflected not only in their size but also in their structure and material properties, may be important for mechanisms of health and disease that are associated with amyloid fibrils.

ASSOCIATED CONTENT

Supporting Information

The Supporting Information is available free of charge on the ACS Publications website at DOI: 10.1021/acs.jctc.5b00657.

Details of simulations (S1), replica-exchange simulation analysis details (S2), calculation of osmotic pressure in CG sorbitol (S3), calculation of preferential interaction of sorbitol with peptide (S4), details about peptide SASA changes in the presence of sorbitol (S5), the kinetic model used to fit experimental and simulation results (S6), and appendices 1, 2 and 3 that detail MARTINI parameters used for the peptide and sorbitol model, respectively (PDF)

AUTHOR INFORMATION

Corresponding Author

*E-mail: daniel@fh.huji.ac.il

Present Address

[†]Department of Chemistry, University of Illinois, Urbana, IL 61801, USA.

Notes

The authors declare no competing financial interest.

ACKNOWLEDGMENTS

We thank B. Hirshberg for help with Gaussian software calculations. Financial support from the Israel Science Foundation (ISF Grant No. 1538/13) is gratefully acknowledged. We acknowledge the European Soft Matter Infrastructure (ESMI, grant No. C120500239) for computational time awarded to S.S. on the JuROPA HPC. L.S is supported by the Adams Fellowship Program of the Israel Academy of Sciences and Humanities. The Fritz Haber Research Center is supported by the Minerva Foundation, Munich, Germany.

REFERENCES

- (1) Dobson, C. M. Protein Folding and Misfolding. *Nature* **2003**, *426*, 884–890.
- (2) Goldschmidt, L.; Teng, P. K.; Riek, R.; Eisenberg, D. Identifying the Amylome, Proteins Capable of Forming Amyloid-like Fibrils. *Proc. Natl. Acad. Sci. U. S. A.* **2010**, *107*, 3487–3492.
- (3) Cherny, I.; Gazit, E. Amyloids: Not Only Pathological Agents but Also Ordered Nanomaterials. *Angew. Chem., Int. Ed.* **2008**, *47*, 4062–4069.
- (4) Winner, B.; Jappelli, R.; Maji, S. K.; Desplats, P. A.; Boyer, L.; Aigner, S.; Hetzer, C.; Loher, T.; Vilar, M.; Campioni, S.; Tzitzilonis, C.; Soragni, A.; Jessberger, S.; Mira, H.; Consiglio, A.; Pham, E.; Masliah, E.; Gage, F. H.; Riek, R. In Vivo Demonstration That α -Synuclein Oligomers Are Toxic. *Proc. Natl. Acad. Sci. U. S. A.* **2011**, *108*, 4194–4199.
- (5) Chimon, S.; Shaibat, M. A.; Jones, C. R.; Calero, D. C.; Aizezi, B.; Ishii, Y. Evidence of Fibril-like β -Sheet Structures in a Neurotoxic Amyloid Intermediate of Alzheimer's β -Amyloid. *Nat. Struct. Mol. Biol.* **2007**, *14*, 1157–1164.
- (6) Stanley, C. B.; Perevozchikova, T.; Berthelie, V. Structural Formation of Huntingtin Exon 1 Aggregates Probed by Small-Angle Neutron Scattering. *Biophys. J.* **2011**, *100*, 2504–2512.
- (7) Arakawa, T.; Timasheff, S. N. The Stabilization of Proteins by Osmolytes. *Biophys. J.* **1985**, *47*, 411–414.
- (8) Yancey, P. H.; Clark, M. E.; Hand, S. C.; Bowlus, R. D.; Somero, G. N. Living with Water Stress: Evolution of Osmolyte Systems. *Science* **1982**, *217*, 1214–1222.
- (9) Bandyopadhyay, A.; Saxena, K.; Kasturia, N.; Dalal, V.; Bhatt, N.; Rajkumar, A.; Maity, S.; Sengupta, S.; Chakraborty, K. Chemical Chaperones Assist Intracellular Folding to Buffer Mutational Variations. *Nat. Chem. Biol.* **2012**, *8*, 238–245.
- (10) Auton, M.; Rösger, J.; Sinev, M.; Holthausen, L. M. F.; Bolen, D. W. Effects on Protein Stability and Solubility: A Balancing Act between Backbone and Side-Chains. *Biophys. Chem.* **2011**, *159*, 90–99.
- (11) Sarkar, M.; Lu, J.; Pielak, G. J. Protein Crowder Charge and Protein Stability. *Biochemistry* **2014**, *53*, 1601–1606.
- (12) Levy-Sakin, M.; Berger, O.; Feibish, N.; Sharon, N.; Schnaider, L.; Shmul, G.; Amir, Y.; Buzhansky, L.; Gazit, E. The Influence of Chemical Chaperones on Enzymatic Activity under Thermal and Chemical Stresses: Common Features and Variation among Diverse Chemical Families. *PLoS One* **2014**, *9*, e88541.
- (13) Yancey, P. H. Water Stress, Osmolytes and Proteins. *Am. Zool.* **2001**, *41*, 699–709.
- (14) Burg, M. B.; Ferraris, J. D.; Dmitrieva, N. I. Cellular Response to Hyperosmotic Stresses. *Physiol. Rev.* **2007**, *87*, 1441–1474.

- (15) Nayak, A.; Lee, C.-C.; McRae, G. J.; Belfort, G. Osmolyte Controlled Fibrillation Kinetics of Insulin: New Insight into Fibrillation Using the Preferential Exclusion Principle. *Biotechnol. Prog.* **2009**, *25*, 1508–1514.
- (16) McLaurin, J.; Golomb, R.; Jurewicz, a; Antel, J. P.; Fraser, P. E. Inositol Stereoisomers Stabilize an Oligomeric Aggregate of Alzheimer Amyloid β Peptide and Inhibit $\alpha\beta$ -Induced Toxicity. *J. Biol. Chem.* **2000**, *275*, 18495–18502.
- (17) Ignatova, Z.; Gierasch, L. M. Inhibition of Protein Aggregation in Vitro and in Vivo by a Natural Osmoprotectant. *Proc. Natl. Acad. Sci. U. S. A.* **2006**, *103*, 13357–13361.
- (18) McLaurin, J.; Kierstead, M. E.; Brown, M. E.; Hawkes, C. a; Lambermon, M. H. L.; Phinney, A. L.; Darabie, A. A.; Cousins, J. E.; French, J. E.; Lan, M. F.; Chen, F.; Wong, S. S. N.; Mount, H. T. J.; Fraser, P. E.; Westaway, D., St; George-Hyslop, P. Cyclohexanehexol Inhibitors of $\alpha\beta$ Aggregation Prevent and Reverse Alzheimer Phenotype in a Mouse Model. *Nat. Med.* **2006**, *12*, 801–808.
- (19) Sukenik, S.; Harries, D. Insights into the Disparate Action of Osmolytes and Macromolecular Crowders on Amyloid Formation. *Prion* **2012**, *6*, 26–31.
- (20) Thirumalai, D.; Reddy, G.; Straub, J. E. Role of Water in Protein Aggregation and Amyloid Polymorphism. *Acc. Chem. Res.* **2012**, *45*, 83–92.
- (21) Macchi, F.; Eisenkolb, M.; Kiefer, H.; Otzen, D. E. The Effect of Osmolytes on Protein Fibrillation. *Int. J. Mol. Sci.* **2012**, *13*, 3801–3819.
- (22) Hamley, I. W.; Nutt, D. R.; Brown, G. D.; Miravet, J. F.; Escuder, B.; Rodríguez-Llansola, F. Influence of the Solvent on the Self-Assembly of a Modified Amyloid β Peptide Fragment. II. NMR and Computer Simulation Investigation. *J. Phys. Chem. B* **2010**, *114*, 940–951.
- (23) Sukenik, S.; Politi, R.; Ziserman, L.; Danino, D.; Friedler, A.; Harries, D. Crowding Alone Cannot Account for Cosolute Effect on Amyloid Aggregation. *PLoS One* **2011**, *6*, e15608.
- (24) Knowles, T. P. J.; Waudby, C. A.; Devlin, G. L.; Cohen, S. I. A.; Aguzzi, A.; Vendruscolo, M.; Terentjev, E. M.; Welland, M. E.; Dobson, C. M. An Analytical Solution to the Kinetics of Breakable Filament Assembly. *Science* **2009**, *326*, 1533–1537.
- (25) Bieler, N. S.; Knowles, T. P. J.; Frenkel, D.; Vácha, R. Connecting Macroscopic Observables and Microscopic Assembly Events in Amyloid Formation Using Coarse Grained Simulations. *PLoS Comput. Biol.* **2012**, *8*, e1002692.
- (26) Morriss-Andrews, A.; Shea, J.-E. Simulations of Protein Aggregation: Insights from Atomistic and Coarse-Grained Models. *J. Phys. Chem. Lett.* **2014**, *5*, 1899–1908.
- (27) Friedman, R. Aggregation of Amyloids in a Cellular Context: Modelling and Experiment. *Biochem. J.* **2011**, *438*, 415–426.
- (28) Kelley, N. W.; Vishal, V.; Krafft, G. A.; Pande, V. S. Simulating Oligomerization at Experimental Concentrations and Long Time-scales: A Markov State Model Approach. *J. Chem. Phys.* **2008**, *129*, 214707.
- (29) Latshaw, D. C.; Cheon, M.; Hall, C. K. Effects of Macromolecular Crowding on Amyloid Beta (16–22) Aggregation Using Coarse-Grained Simulations. *J. Phys. Chem. B* **2014**, *118*, 13513–13526.
- (30) O'Brien, E. P.; Straub, J. E.; Brooks, B. R.; Thirumalai, D. Influence of Nanoparticle Size and Shape on Oligomer Formation of an Amyloidogenic Peptide. *J. Phys. Chem. Lett.* **2011**, *2*, 1171–1177.
- (31) Li, X.; Mehler, E. L. Simulation of Molecular Crowding Effects on an Alzheimer's β -Amyloid Peptide. *Cell Biochem. Biophys.* **2006**, *46*, 123–142.
- (32) Cheon, M.; Chang, I.; Mohanty, S.; Luheshi, L. M.; Dobson, C. M.; Vendruscolo, M.; Favrin, G. Structural Reorganisation and Potential Toxicity of Oligomeric Species Formed during the Assembly of Amyloid Fibrils. *PLoS Comput. Biol.* **2007**, *3*, 1727–1738.
- (33) Bereau, T.; Deserno, M. Generic Coarse-Grained Model for Protein Folding and Aggregation. *J. Chem. Phys.* **2009**, *130*, 235106.
- (34) Latshaw, D. C.; Hall, C. K. Effects of Hydrophobic Macromolecular Crowders on Amyloid β (16–22) Aggregation. *Biophys. J.* **2015**, *109*, 124–134.
- (35) Marrink, S.-J.; Risselada, H. J.; Yefimov, S.; Tieleman, D. P.; de Vries, A. H. The MARTINI Force Field: Coarse Grained Model for Biomolecular Simulations. *J. Phys. Chem. B* **2007**, *111*, 7812–7824.
- (36) Monticelli, L.; Kandasamy, S. K.; Periole, X.; Larson, R. G.; Tieleman, D. P.; Marrink, S.-J. The MARTINI Coarse-Grained Force Field: Extension to Proteins. *J. Chem. Theory Comput.* **2008**, *4*, 819–834.
- (37) Marrink, S. J.; Tieleman, D. P. Perspective on the Martini Model. *Chem. Soc. Rev.* **2013**, *42*, 6801.
- (38) Maynard, A. J.; Sharman, G. J.; Searle, M. S. Origin of β -Hairpin Stability in Solution: Structural and Thermodynamic Analysis of the Folding of a Model Peptide Supports Hydrophobic Stabilization in Water. *J. Am. Chem. Soc.* **1998**, *120*, 1996–2007.
- (39) Searle, M. S.; Griffiths-Jones, S. R.; Skinner-Smith, H. Energetics of Weak Interactions in a β -Hairpin Peptide: Electrostatic and Hydrophobic Contributions to Stability from Lysine Salt Bridges. *J. Am. Chem. Soc.* **1999**, *121*, 11615–11620.
- (40) Sukenik, S.; Sapir, L.; Gilman-Politi, R.; Harries, D. Diversity in the Mechanisms of Cosolute Action on Biomolecular Processes. *Faraday Discuss.* **2013**, *160*, 225.
- (41) Sukenik, S.; Sapir, L.; Harries, D. Balance of Enthalpy and Entropy in Depletion Forces. *Curr. Opin. Colloid Interface Sci.* **2013**, *18*, 495–501.
- (42) Sukenik, S.; Boyarski, Y.; Harries, D. Effect of Salt on the Formation of Salt-Bridges in β -Hairpin Peptides. *Chem. Commun.* **2014**, *50*, 8193–8196.
- (43) Politi, R.; Harries, D. Enthalpically Driven Peptide Stabilization by Protective Osmolytes. *Chem. Commun.* **2010**, *46*, 6449–6451.
- (44) Gilman-Politi, R.; Harries, D. Unraveling the Molecular Mechanism of Enthalpy Driven Peptide Folding by Polyol Osmolytes. *J. Chem. Theory Comput.* **2011**, *7*, 3816–3828.
- (45) Seo, M.; Rauscher, S.; Pomès, R.; Tieleman, D. P. Improving Internal Peptide Dynamics in the Coarse-Grained MARTINI Model: Toward Large-Scale Simulations of Amyloid- and Elastin-like Peptides. *J. Chem. Theory Comput.* **2012**, *8*, 1774–1785.
- (46) Kirschner, K. N.; Yongye, A. B.; Tschampel, S. M.; González-Outeiriño, J.; Daniels, C. R.; Foley, B. L.; Woods, R. J. GLYCAM06: A Generalizable Biomolecular Force Field. *Carbohydrates. J. Comput. Chem.* **2008**, *29*, 622–655.
- (47) Hu, Y.; Zhang, Z.-X.; Zhang, Y.; Fan, S.; Liang, D. Viscosity and Density of the Nonelectrolyte System Mannitol + Sorbitol + Sucrose + H₂O and Its Binary and Ternary Subsystems at 298.15 K. *J. Chem. Eng. Data* **2006**, *51*, 438–442.
- (48) Kirkwood, J. G.; Buff, F. P. The Statistical Mechanical Theory of Solutions. I. *J. Chem. Phys.* **1951**, *19*, 774.
- (49) Harries, D.; Rösgen, J. A Practical Guide on How Osmolytes Modulate Macromolecular Properties. *Methods Cell Biol.* **2008**, *84*, 679–735.
- (50) Rösgen, J. Molecular Basis of Osmolyte Effects on Protein and Metabolites. *Methods Enzymol.* **2007**, *428*, 459–486.
- (51) Mukherji, D.; van der Vegt, N. F. A.; Kremer, K.; Delle Site, L. Kirkwood–Buff Analysis of Liquid Mixtures in an Open Boundary Simulation. *J. Chem. Theory Comput.* **2012**, *8*, 375–379.
- (52) Rösgen, J.; Pettitt, B. M.; Bolen, D. W. An Analysis of the Molecular Origin of Osmolyte-Dependent Protein Stability. *Protein Sci.* **2007**, *16*, 733–743.
- (53) Greene, R. F.; Pace, C. N. Urea and Guanidine Hydrochloride Denaturation of Ribonuclease, Lysozyme, α -Chymotrypsin, and β -Lactoglobulin. *J. Biol. Chem.* **1974**, *249*, 5388–5393.
- (54) Hu, C. Y.; Kokubo, H.; Lynch, G. C.; Bolen, D. W.; Pettitt, B. M. Backbone Additivity in the Transfer Model of Protein Solvation. *Protein Sci.* **2010**, *19*, 1011–1022.
- (55) Liu, Y. F.; Bolen, D. W. The Peptide Backbone Plays a Dominant Role in Protein Stabilization by Naturally-Occurring Osmolytes. *Biochemistry* **1995**, *34*, 12884–12891.

- (56) Grossfield, A.; Zuckerman, D. M. Quantifying Uncertainty and Sampling Quality in Biomolecular Simulations. *Annu. Rep. Comput. Chem.* **2009**, *5*, 23–48.
- (57) Pronk, S.; Páll, S.; Schulz, R.; Larsson, P.; Bjelkmar, P.; Apostolov, R.; Shirts, M. R.; Smith, J. C.; Kasson, P. M.; Van Der Spoel, D.; Hess, B.; Lindahl, E. GROMACS 4.5: A High-Throughput and Highly Parallel Open Source Molecular Simulation Toolkit. *Bioinformatics* **2013**, *29*, 845–854.
- (58) Jiang, X.; Zhu, C.; Ma, Y. Density and Viscosity of Sorbitol/maltitol in L-Ascorbic Acid Aqueous Solutions at T = (293.15 to 323.15)K. *J. Mol. Liq.* **2013**, *188*, 67–73.
- (59) Cho, S. S.; Levy, Y.; Wolynes, P. G. P versus Q: Structural Reaction Coordinates Capture Protein Folding on Smooth Landscapes. *Proc. Natl. Acad. Sci. U. S. A.* **2006**, *103*, 586–591.
- (60) Stark, A. C.; Andrews, C. T.; Elcock, A. H. Toward Optimized Potential Functions for Protein–Protein Interactions in Aqueous Solutions: Osmotic Second Virial Coefficient Calculations Using the MARTINI Coarse-Grained Force Field. *J. Chem. Theory Comput.* **2013**, *9*, 4176–4185.
- (61) Nishizawa, M.; Nishizawa, K. Potential of Mean Force Analysis of the Self-Association of Leucine-Rich Transmembrane α -Helices: Difference between Atomistic and Coarse-Grained Simulations. *J. Chem. Phys.* **2014**, *141*, 075101.
- (62) Hatters, D. M.; Minton, A. P.; Howlett, G. J. Macromolecular Crowding Accelerates Amyloid Formation by Human Apolipoprotein C-II. *J. Biol. Chem.* **2002**, *277*, 7824–7830.
- (63) Zhou, H.-X.; Rivas, G.; Minton, A. P. Macromolecular Crowding and Confinement: Biochemical, Biophysical, and Potential Physiological Consequences. *Annu. Rev. Biophys.* **2008**, *37*, 375–397.
- (64) Munishkina, L. A.; Ahmad, A.; Fink, A. L.; Uversky, V. N. Guiding Protein Aggregation with Macromolecular Crowding. *Biochemistry* **2008**, *47*, 8993–9006.
- (65) White, D. A.; Buell, A. K.; Knowles, T. P. J.; Welland, M. E.; Dobson, C. M. Protein Aggregation in Crowded Environments. *J. Am. Chem. Soc.* **2010**, *132*, 5170–5175.
- (66) Shoemaker, B. A.; Portman, J. J.; Wolynes, P. G. Speeding Molecular Recognition by Using the Folding Funnel: The Fly-Casting Mechanism. *Proc. Natl. Acad. Sci. U. S. A.* **2000**, *97*, 8868–8873.
- (67) Nguyen, P. H.; Li, M. S.; Stock, G.; Straub, J. E.; Thirumalai, D. Monomer Adds to Preformed Structured Oligomers of $\alpha\beta$ -Peptides by a Two-Stage Dock-Lock Mechanism. *Proc. Natl. Acad. Sci. U. S. A.* **2007**, *104*, 111–116.
- (68) Rösgen, J.; Pettitt, B. M.; Bolen, D. W. Protein Folding, Stability, and Solvation Structure in Osmolyte Solutions. *Biophys. J.* **2005**, *89*, 2988–2997.
- (69) Courtenay, E. S.; Capp, M. W.; Saecker, R. M.; Record, M. T., Jr. Thermodynamic Analysis of Interactions Between Denaturants and Protein Surface Exposed on Unfolding: Interpretation of Urea and Guanidinium Chloride *m*-Values and Their Correlation with Changes in Accessible Surface Area (ASA) Using Preferential Interaction Coefficients and the Local-Bulk Domain Model. *Proteins: Struct., Funct., Genet.* **2000**, *41*, 72–85.
- (70) Holthauzen, L. M. F.; Bolen, D. W. Mixed Osmolytes: The Degree to Which One Osmolyte Affects the Protein Stabilizing Ability of Another. *Protein Sci.* **2007**, *16*, 293–298.
- (71) Canchi, D. R.; García, A. E. Cosolvent Effects on Protein Stability. *Annu. Rev. Phys. Chem.* **2013**, *64*, 273–293.
- (72) Miller, Y.; Ma, B.; Nussinov, R. Polymorphism in Alzheimer A β Amyloid Organization Reflects Conformational Selection in a Rugged Energy Landscape. *Chem. Rev.* **2010**, *110*, 4820–4838.
- (73) Colletier, J.; Laganowsky, A.; Landau, M.; Zhao, M.; Soriaga, A. B.; Goldschmidt, L.; Flot, D.; Cascio, D.; Sawaya, M. R.; Eisenberg, D. Molecular Basis for Amyloid- β Polymorphism. *Proc. Natl. Acad. Sci. U. S. A.* **2011**, *108*, 16938–16943.
- (74) Ha, C.; Park, C. B. Template-Directed Self-Assembly and Growth of Insulin Amyloid Fibrils. *Biotechnol. Bioeng.* **2005**, *90*, 848–855.
- (75) Arimon, M.; Sanz, F.; Giralt, E.; Carulla, N. Template-Assisted Lateral Growth of Amyloid- β 42 Fibrils Studied by Differential Labeling with Gold Nanoparticles. *Bioconjugate Chem.* **2012**, *23*, 27–32.
- (76) Margittai, M.; Langen, R. Template-Assisted Filament Growth by Parallel Stacking of Tau. *Proc. Natl. Acad. Sci. U. S. A.* **2004**, *101*, 10278–10283.
- (77) Candotti, M.; Esteban-Martín, S.; Salvatella, X.; Orozco, M. Toward an Atomistic Description of the Urea-Denatured State of Proteins. *Proc. Natl. Acad. Sci. U. S. A.* **2013**, *110*, 5933–5938.